Accepted for publication in ApJ
Preprint typeset using LaTeX style emulateapj v. 01/23/15

arXiv:1604.00015v2 [astro-ph.GA] 5 Aug 2016

SWIFT COALESCENCE OF SUPERMASSIVE BLACK HOLES IN COSMOLOGICAL MERGERS OF MASSIVE GALAXIES

Fazeel Mahmood Khan[1], Davide Fiacconi[2], Lucio Mayer[2], Peter Berczik[3,4,5], and Andreas Just[5]

Accepted for publication in ApJ

ABSTRACT

Supermassive black holes (SMBHs) are ubiquitous in galaxies with a sizable mass. It is expected that a pair of SMBHs originally in the nuclei of two merging galaxies would form a binary and eventually coalesce via a burst of gravitational waves. So far theoretical models and simulations have been unable to predict directly the SMBH merger timescale from ab-initio galaxy formation theory, focusing only on limited phases of the orbital decay of SMBHs under idealized conditions of the galaxy hosts. The predicted SMBH merger timescales are long, of order Gyrs, which could be problematic for future gravitational wave searches. Here we present the first multi-scale ΛCDM cosmological simulation that follows the orbital decay of a pair of SMBHs in a merger of two typical massive galaxies at $z \sim 3$, all the way to the final coalescence driven by gravitational wave emission. The two SMBHs, with masses $\sim 10^8$ $M_\odot$, settle quickly in the nucleus of the merger remnant. The remnant is triaxial and extremely dense due to the dissipative nature of the merger and the intrinsic compactness of galaxies at high redshift. Such properties naturally allow a very efficient hardening of the SMBH binary. The SMBH merger occurs in only ~ 10 Myr after the galactic cores have merged, which is two orders of magnitude smaller than the Hubble time.

Keywords: black hole physics – galaxies: interactions – galaxies: kinematics and dynamics – galaxies: nuclei – gravitational waves – methods: numerical

1. INTRODUCTION

Dual active galactic nuclei (AGNs) at kiloparsec to hundred parsec separations have been detected (Comerford et al. 2013), but at smaller separations there are only unconfirmed candidates (Eracleous et al. 2012; Graham et al. 2015). At the same time, the orbital decay of two supermassive black holes (SMBHs) at the center of merging galaxies (Begelman et al. 1980) has been theoretically studied with a variety of computer simulations, but always neglecting one or more important processes. Substantial work has focused on the gravitational interaction between the SMBHs and the stellar background, as it would be appropriate for a gas-free galaxy (Makino & Funato 2004; Vasiliev et al. 2015), as well as on the dynamics of two SMBHs within a dissipative gaseous background, though neglecting gravitational encounters with individual stars (Dotti et al. 2007; Mayer et al. 2007; Chapon et al. 2013). Furthermore, individual simulations, due to computational limitations, typically follow only a limited phase of the SMBH pair evolution, either before or after a Keplerian binary forms (Mayer 2013). It has been noticed that SMBHs in stellar systems may stall at parsec separations as the loss cone is depleted, rendering the transfer of energy between the binary and the stellar background inefficient (Makino & Funato 2004; Berczik et al. 2005). This has been dubbed the "last parsec problem" (Milosavljević & Merritt 2001). However, it has been shown that the loss cone can be refilled if the potential of the galaxy has substantial deviations from sphericity (Khan et al. 2011; Preto et al. 2011; Vasiliev et al. 2015). Yet, extrapolating the hardening rates seen in these recent simulations to the gravitational wave (GW) dominated phase using analytical models, the resulting SMBH merger timescales are ~ 1 Gyr (Khan et al. 2012a,b). The galaxy merger timescale is also of order a Gyr (Stewart et al. 2009), suggesting that the overall process takes a significant fraction of the age of the Universe. At $z > 2$, when the lookback time is also of order a few Gyr, this would imply low SMBH coalescence rates, a potential problem for future GW experiments such as the Evolved Laser Interferometer Space Antenna (eLISA) (Amaro-Seoane et al. 2013).

If gas is present, such as in circumnuclear disks forming as a result of gas-rich mergers, the orbital decay of the SMBHs proceeds on a faster track, leading to a hard binary with pc-scale separation in $\sim 1 - 100$ Myr, depending on the clumpiness of the interstellar medium (Mayer et al. 2007; Chapon et al. 2013; Fiacconi et al. 2013; Roškar et al. 2015). However, the drag may become inefficient at smaller separations, potentially resulting in a stalling binary (Chapon et al. 2013; Mayer 2013).

The results of all these simulations depend strongly on the mass distribution and properties of the stars and interstellar gas of the circumnuclear region, which are inherited from idealized initial conditions. Therefore it is still unclear how and at what pace the orbital decay of

khanfazeel.ist@gmail.com
[1] Department of Space Science, Institute of Space Technology, PO Box 2750 Islamabad, Pakistan
[2] Center for Theoretical Astrophysics and Cosmology, Institute for Computational Science, University of Zurich, Winterthurerstrasse 190, CH-8057 Zürich, Switzerland
[3] National Astronomical Observatories and Key Laboratory of Computational Astrophysics, Chinese Academy of Sciences, 20A Datun Rd., Chaoyang District, 100012, Beijing, China
[4] Main Astronomical Observatory, National Academy of Sciences of Ukraine, 27 Akademika Zabolotnoho St., 03680, Kyiv, Ukraine
[5] Astronomisches Rechen-Institut, Zentrum für Astronomie der Universität Heidelberg, Mönchhofstrasse 12-14, 69120, Heidelberg, Germany

SMBHs proceeds in realistic galaxy mergers. In order to make progress, in this paper we have carried out the first ab-initio calculation of a SMBH merger that starts from a galaxy merger pinpointed in a state-of-the-art cosmological hydrodynamical simulation. We follow the SMBHs all the way to the final spiral-in phase with the aid of post-Newtonian corrections (Blanchet 2006).

2. GALAXY MERGER SIMULATION

We identify the merger of two massive galaxies at $z \sim 3.5$ in the Argo cosmological hydrodynamical simulation (Feldmann & Mayer 2015; Fiacconi et al. 2015). The simulation follows the formation of a group-sized halo with mass $\approx 2 \times 10^{13}$ M$_\odot$ at $z = 0$, and includes gas cooling, star formation (SF) and a supernovae feedback models that have been shown to produce realistic galaxies at a variety of mass scales (Governato et al. 2010; Guedes et al. 2011). The halo evolves in a mildly over-dense region and its virial mass is close to the characteristic scale $M^\star$ of the halo mass function at low z, suggesting that it should be a common host for massive galaxies (Feldmann & Mayer 2015; Fiacconi et al. 2015). In lower resolution simulations the group hosts a central galaxy with properties typical of massive early-types at $z = 0$ (Feldmann et al. 2010).

The central galaxy of the Argo simulation undergoes its last major merger (with a stellar mass ratio ~ 0.3) at $z \simeq 3.5$. The merger involves two disk-like galaxies in a nearly parabolic (slightly hyperbolic) orbit, with their stellar spins misaligned by $\approx 67°$. Such a configuration is typical for major mergers in ΛCDM cosmology (Khochfar & Burkert 2006). The two galaxies have stellar masses $M_{\star,1} \approx 3.6 \times 10^{10}$ M$_\odot$ and $M_{\star,2} \approx 10^{10}$ M$_\odot$, and gas fractions $f_1 \approx 7.7\%$ and $f_2 = 11.5\%$, respectively. The two galaxies and their group environment are shown in Figure 1 when they are about to merge.

The cosmological simulation does not originally contain any SMBH, and its resolution would not allow us to probe the evolution of a BH binary. Therefore, we increase the resolution by performing static particle splitting (Mayer et al. 2007; Roškar et al. 2015). Specifically, we extract from the cosmological simulation a spherical region with radius ~ 13.5 kpc at $z = 3.6$ that encompasses the two galaxies and part of their environment. We check that the average dynamical time of such region is $\gtrsim 100$ Myr, which is larger than the dynamical time in the central region and the simulation time that we target, about a few tens of Myr. At this stage, the cores of the two galaxies are at a separation of $\lesssim 4$ kpc. We then split all particle species in 8 child particles with masses 8 times smaller and the same velocity of the parent particle, thus conserving mass and linear momentum exactly, and angular momentum at the kernel level. Thermodynamic properties of gas particles (i.e. density and temperature) are interpolated among the child particles (Roškar et al. 2015), while child stellar particles maintain the properties of their parents (e.g. the age). After the splitting, the simulation contains 9 452 581 stellar particles, 1 088 920 gas particles, and 1 669 922 dark matter particles with masses 6.4×10^3 M$_\odot$, 2×10^4 M$_\odot$, and 10^5 M$_\odot$, respectively. We reduce to $\epsilon = 5$ pc the gravitational softenings[6] of gaseous and stellar particles to increase the spatial resolution, while the dark matter softening is reduced by a factor $8^{1/3} = 2$ to maintain the local density and the smooth gravitational field. We extensively tested this procedure by running twin simulations with $\epsilon = 15$ and 50 pc; we checked that (i) no spurious effects on scales larger than the original softening were introduced, and (ii) the dynamics of the introduced SMBHs (see below) converged down to the adopted softenings (see Section A for quantitative details).

During the splitting procedure, we introduce two SMBHs at the local minima of the gravitational potential of the galactic cores. We assign to the SMBHs the mass-weighted average velocity of all the particles within 250 pc from their positions. We checked that the velocities do not depend strongly on the size of the regions that we choose. Since the two galaxies are relatively gas-poor at $z \sim 3.5$ and we aim to continue the simulation for $\sim 20 - 40$ Myr, we neglect mass accretion and feedback from the SMBHs, that are thus treated as collisionless particles. The SMBHs have the same softening as stellar and gas particles. We finally choose their masses according to local scaling relations (Ferrarese & Merritt 2000; Tremaine et al. 2002; McConnell & Ma 2013; Scott et al. 2013; Kormendy & Ho 2013). We used (McConnell & Ma 2013) to determine the SMBH masses after measuring the average velocity dispersion within one half-mass radius for each galaxy before performing particle splitting. The resulting masses are $M_{\bullet,1} = 3 \times 10^8$ M$_\odot$ and $M_{\bullet,2} = 8 \times 10^7$ M$_\odot$, with a mass ratio $M_{\bullet,1}/M_{\bullet,2} = 3.75$. Though using the local scaling relations for the SMBH masses is formally inappropriate for high-z galaxies, this might result to be a conservative choice because there are both observational (Merloni et al. 2010; Trakhtenbrot et al. 2015) and theoretical (DeGraf et al. 2015) hints that the normalization of those relations increases at high-z, i.e. galaxies host proportionally larger SMBHs.

After setting-up the initial conditions as described, we simulate the final stages of the galaxy merger until the separation of the two SMBHs is about the resolution. We use the GASOLINE code (Wadsley et al. 2004), but including additional sub-resolution physics. Specifically, we add the gas radiative cooling from metal lines, a pressure floor to avoid spurious fragmentation, and an equilibrium temperature-density relation for gas denser than 0.1 H cm^{-3} to model the optically-thick phase, calibrated on 2D radiative transfer simulations in typical starburst conditions (Spaans & Silk 2000; Roškar et al. 2015). We also increase the density threshold to form star to 1000 H cm^{-3} and we reduce the temperature threshold to 300 K, to account for the new cooling.

Figure 2 shows different stages of the merger of the two galaxies in our simulation after we perform the particle splitting. The Figure reveals that the two galaxies are flattened and disk-like. The remnant has an elongated shape out to a few kpc soon after the merger.

3. SUPERMASSIVE BLACK HOLE BINARY EVOLUTION

The left panel of Figure 3 describes the orbital evolution of the two SMBHs starting form ~ 4 kpc till the final coalescence. As the two galaxies merge, their SMBHs sink in the remnant surrounded by stellar cusps bound

[6] The gravitational softenings of the Argo simulation are 120 pc and 250 pc for baryons and dark matter, respectively.

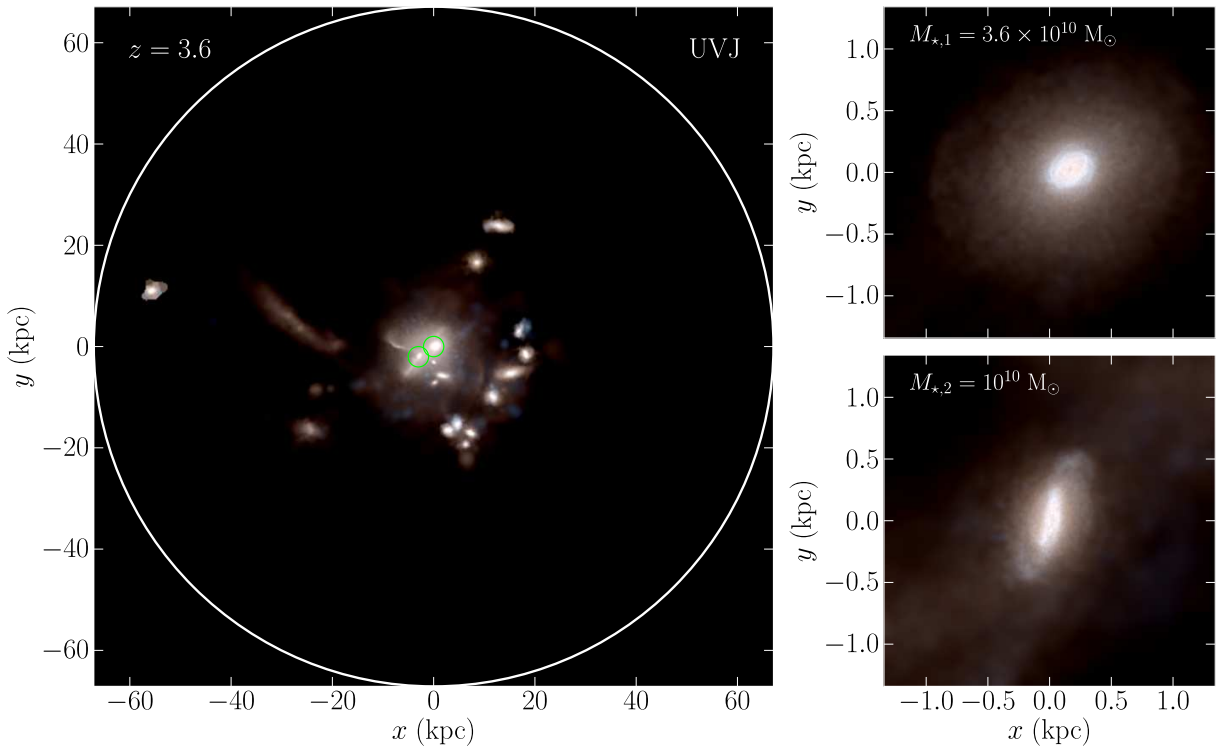

Figure 1. Group environment of the galaxy merger. The left panel shows a mock UVJ map of the galaxy group at $z = 3.6$. The white circle marks the virial radius of the group halo, while the green circles mark the merging galaxies. The upper-right and lower-right panels show a zoom-in on the central galaxy of the group and the interacting companion, respectively. Lengths are in physical coordinates.

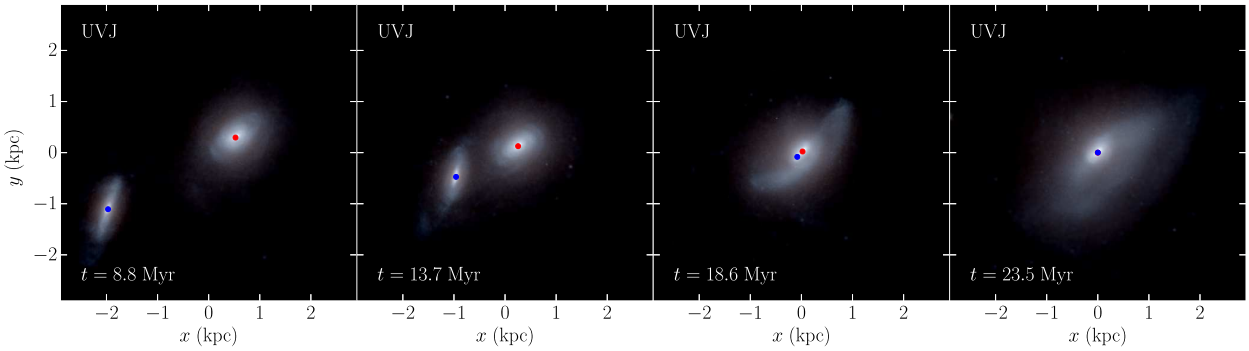

Figure 2. From left to right: time evolution of the galaxy merger after the beginning of the re-sampled, higher-resolution simulation. Each panel shows a mock UVJ photometric image of the merger, and the red and blue dots mark the position of the primary and secondary BH, respectively. Lengths are in physical coordinates.

to them. The orbital decay is governed by dynamical friction of the stellar cusps against the stellar, gas and dark matter background originating from the merger of the two hosts.

During the final stage of the merger (i.e. at $t \approx 20$ Myr after the particle splitting) the merger remnant is gas poor (gas fraction $\sim 5\%$) owing to gas consumption by SF. Stars dominate the enclosed mass out to ~ 3 kpc and provide the dominant contribution to the dynamical friction exerted by the background. Figure 4 shows the mass distribution of the individual components when the separation of the two SMBHs reaches about 300 pc, i.e. ≈ 21.5 Myr after the particle splitting. The stellar mass is almost 2 orders of magnitude larger than the gas one over all spatial scales except in the central 10 pc, where the difference is about a factor of 20.

Then, we extract a spherical region of 5 kpc at $t \sim 21.5$ Myr after particle splitting around the more massive SMBH to initialize a direct N-body simulation containing in total $\sim 6 \times 10^6$ particles. We treat the remaining gas particles in the selected volume as stars, since they are sub-dominant in mass. Almost the entire stellar mass is within 5 kpc, so an artificial cut-off at 5 kpc shall not introduce significant changes in stellar mass profile in the inner region for follow up evolution. However, at truncation separation, the dark matter has a steeply rising

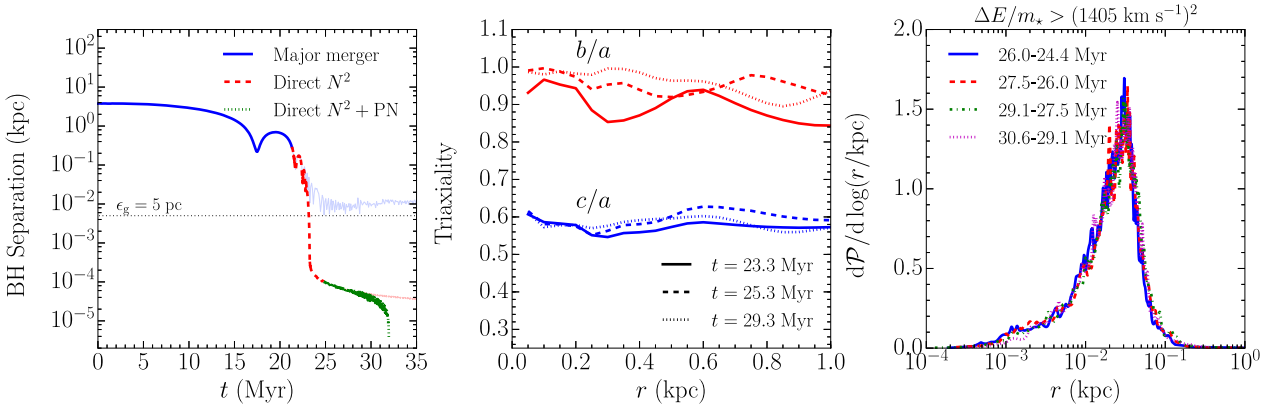

Figure 3. Left panel: time evolution of the separation between the SMBHs. Blue-solid, red-dashed, and green-dotted lines show the evolution during the hydrodynamical, re-sampled simulation of the merger, the direct N-body calculation, and after having introduced post-Newtonian corrections, respectively. Thin and light versions of the same lines refer to the continuation of the respective simulations. The horizontal dotted line marks the gravitational softening of the hydrodynamical simulation. Central panel: radial profiles of the ratio b/a (red) and c/a (blue) between the principal axes of the moment of inertia tensor ($c \leq b \leq a$) at different times: 23.3 Myr (solid), 25.3 Myr (dashed), and 29.3 Myr (dotted). Right panel: probability density function of the radial distance from the center of the merger remnant for the stellar particles that have interacted with the central binary across 26-24.4 Myr (blue, solid), 27.5-26 Myr (red, dashed), 29.1-27.5 Myr (green, dot-dashed), and 30.6-29.1 Myr (magenta, dotted).

mass profile; we compare it with a later snapshot during the N-body evolution at $t \approx 30$ Myr. We do not observe a noticeable evolution from outer to inner region.

We further evolve the selected region using the high-performance ϕ-GPU code (Berczik et al. 2011). At the end of our previous galaxy merger simulation, stellar and gas particles have a softening of 5 pc and dark matter particles have a softening of 150 pc. We start our direct N-body run by decreasing the stellar softening to 0.1 pc while keeping the dark matter particles softening unchanged to avoid two-body relaxation effects as the latter have a relatively large mass. Figure 4 shows that the mass of the dark matter component does not increase in the central region during the whole evolution period. The softening parameter for the force calculation between the two black holes is set to 0. In order to calculate the softening between different particle species we employ the following criterion:

$$\epsilon_{ij}^2 = (\epsilon_i^2 + \epsilon_j^2)/2, \quad (1)$$

where $\epsilon_\bullet = 0$ for both black holes, $\epsilon_\star = 0.1$ pc for stars and $\epsilon_{\rm dm} = 125$ pc for dark matter particles. In star-black hole interactions we further reduce the softening to 0.007 pc, which is smaller than the semi-major axis of the binary when the gravitational wave emission dominates (Figure 3, left panel). In order to take into account energy loss by gravitational wave emission, we incorporate post-newtonian terms up to 3.5 in the equation of motion of the binary SMBHs (Blanchet 2006).

Dynamical friction efficiently shrinks the separation between the two SMBHs and they form a binary once individual cusps merge at $t \sim 23.5$ Myr. The separation drops rapidly to ~ 0.3 pc in less than 1 Myr, owing to the high nuclear density, until the binary gets hard and dynamical friction becomes inefficient. The subsequent phase of the decay is dominated by three-body encounters between the binary and the surrounding stars. This phase is the longest, taking ≈ 8 Myr before the separation decreases to ~ 0.01 pc, at which point GW emission takes over and brings the SMBHs to rapid coalescence in 2 Myr (Figure 3). Figure 3 also shows that post-Newtonian terms are crucial for the sinking of the binary already at a separation of $\gtrsim 0.03$ pc. The orbital decay rate in the post-Newtonian phase is in rough agreement with simple semi-analytical predictions based on orbit-averaged expressions (Peters & Mathews 1963), which do not take into account the contributions from higher order terms.

We define the coalescence time, and stop the simulations, when the separation is $< 4(r_{\rm s,1}+r_{\rm s,2})$, where $r_{{\rm s},j}$ is the Schwarzschild radius of the j-th BH, as following the evolution further would require a fully relativistic treatment. The coalescence, counting from the merger of the two cusps at $t \sim 23.5$ Myr, takes less than 10 Myr, which is roughly two orders of magnitude faster than previous decay time estimates inferred for non-cosmological, purely stellar hosts (when rescaled to nearby galaxies) (Khan et al. 2012b, 2013). The preceding large-scale approach and merger of the two galaxies lasts ~ 200 Myr, so that the overall process is completed in significantly less than the lookback time at $z \sim 3.5$.

The shape of the merger remnant over time is shown in the central panel of Figure 3. It was obtained by measuring the moments of inertia tensor of a homogeneous ellipsoid. The remnant is clearly triaxial at all times. The right panel of Figure 3 shows the distribution of the mean radial distances of the stars that contribute to the change in the binding energy of the binary at different times. Those have been identified statistically as the stars that undergo large specific total energy change between two subsequent snapshots, $\Delta E/m_\star > (1405$ km s$^{-1})^2$. This absolute threshold depends on the binary properties only, $\Delta E/m_\star \approx G\ \mu_\bullet\ C\ a^{-1}$, where $\mu_\bullet$ is the binary reduced mass, a is the binary separation, and $C \approx 2$, as inferred from three-body encounter simulations (Hills 1983; Quinlan 1996). This criterion allows us to select only the stars involved in encounters with the SMBH binary, because the energy changes due to the large scale evolution of the system and to two-body encounters with other stars and dark matter particles are small compared to the adopted threshold. Most of those stars come from 10-100 pc, which is at quite far from the BH binary sitting at the

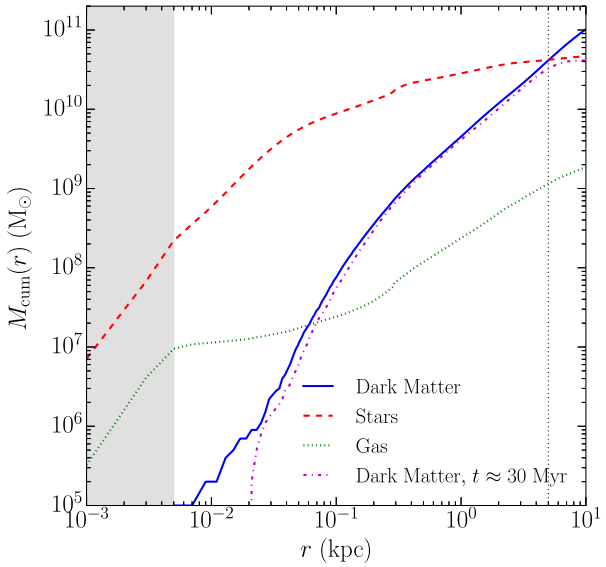

Figure 4. Enclosed mass profile of dark matter (blue, continuous), stars (red, dashed) and gas (green, dotted) at $t \sim 21.5$ Myr when we select the inner 5 kpc (vertical dotted line) for the direct N-body simulation. The gray area marks $\epsilon = 5$ pc. The magenta dot-dashed line shows the dark matter profile at $t \approx 30$ Myr, which is not modified by our truncation.

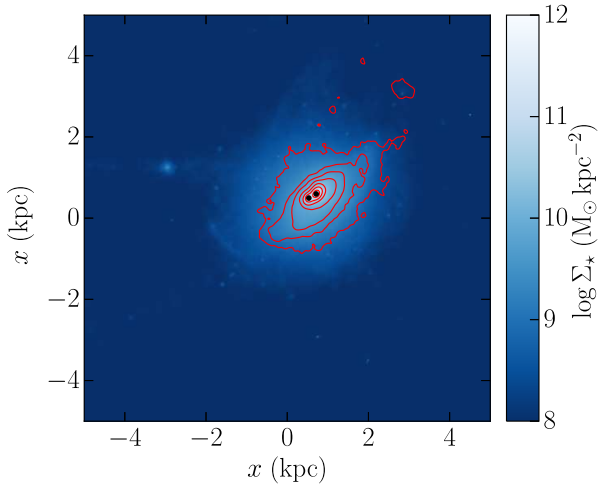

Figure 5. Surface density map of the stellar component at the time of the beginning of the N-body simulation. Red continuous lines represent isocontours of stars younger than ~ 22.5 Myr (i.e. formed from the beginning of the resampled merger simulation) from 5×10^8 to 5×10^{11} $M_\odot$ kpc^{-2} with steps of 0.5 dex. The black dots denote the positions of the two black holes.

center of the remnant. This shows that the loss cone is efficiently refilled from stars on plunging orbits.

Finally, we stress that, at the resolution that we are employing, our results on the binary evolution during the phase dominated by stellar encounters are robust. Indeed, previous tests in flat, rotating, and triaxial systems have shown that the hardening rate is almost independent of the number of particles when above $\sim 10^6$ (Berczik et al. 2006; Khan et al. 2011; Preto et al. 2011; Khan et al. 2013; Holley-Bockelmann & Khan 2015). Since the star particles in our run are $\sim 5.5 \times 10^6$, we expect that we reach a regime of statistical convergence where fewer encounters with more massive particles produce a total energy exchange comparable to that occurring with many more encounters with lighter particles.

4. DISCUSSION AND CONCLUSIONS

In this paper, we discuss the first multi-scale simulation that probes the evolution of a SMBH binary forming within a cosmological major merger, all the way down to the coalescence driven by the emission of GWs. We start from the Argo cosmological simulation, where we identify and re-simulate at higher resolution a major merger between two massive galaxies at $z \approx 3.5$. Gas dissipation before the merger is instrumental in creating the conditions for the rapid orbital decay of the SMBHs, which is our key finding. Indeed, the high central stellar density in the remnant is the result of gas inflows in the inner $\lesssim 500$ pc due to prior cosmological gas accretion and mergers (Feldmann et al. 2010).

These effects cannot be accounted for in idealized galaxy mergers, rather require cosmological simulations as those employed here. The dense remnant not only causes strong dynamical friction by both gas and stars in the early decay phase, but provides an abundant reservoir of stars in the nuclear region that interact with the binary in the late phases of the decay.

At the same time, triaxiality is necessary to avoid the loss cone problem and is a natural result of mergers between non-spherical galaxy progenitors. Since massive galaxies comprise a large fraction of star forming galaxies at high z, many with massive disk-like components (Wisnioski et al. 2015), the pre-merger conditions in our simulation should be typical of the progenitors of massive early-type galaxies that host the most massive SMBHs at low z.

Note that, although we have not included AGN feedback in the simulation, the galaxy merger remnant has an effective radius, central density, and stellar mass that agree well with observations of quiescent high-z massive galaxies (Bezanson et al. 2009; Szomoru et al. 2012; Bezanson et al. 2013), including abundance matching constraints. Indeed, its star formation is efficiently quenched owing to the "cosmological starvation" mechanism described by Feldmann & Mayer (2015).

In order to have an idea how much off our timescales can be by not including AGN feedback, which could suppress star formation, we estimated the density of stars formed during the merger within a sphere of 75 pc radius around the SMBH binary's center of mass. Most stars that interact with binary originate from distances within our chosen region (see figure 3 right panel). Figure 5 shows the total stellar surface density, as well as the contours in red of the surfaces density of the young stars with age below 22.5 Myr, when we switch between the hydro and the direct N-Body calculation. From the Figure it is evinced that new stars form mostly in the central region. We find that newly formed stars only contribute about 8% to the total stellar density which would result in about 8% smaller hardening rates (Sesana & Khan 2015). Hence even if AGN feedback shuts-off star formation completely, it would not cause any significant delay in the swift SMBH merger timescale found in this study.

However AGN feedback could still have a significant effect along earlier branches of the galaxies merger trees on the simulated galaxies prior to the phase when the

galaxy merger begins. While this is beyond the scope of our study, we can get some insight on this by comparing the effective radius of our galaxies with the effective radius of a much larger sample of massive high redshift galaxies, which now includes star forming galaxies rather than only passive quiescent galaxies as in the Bezanson et al. (2009, 2013) work. Such a sample is that of the CANDELS survey (Papovich et al. 2015), which extends to z = 2.8. When compared to the average effective radius of galaxies of the same stellar mass, the effective radius of our simulated galaxies is now about 50% smaller.

This implies that our central stellar densities could be overestimated by a factor of 3, which would result in a SMBH merger timescale about a factor of 3 longer in the slowest phase of the decay, namely hardening due to 3-body encounters. This would imply a merger timescale close to 40 Myr, which would still be almost two order of magnitude shorter than that reported by previous studies (e.g. Khan et al. (2012b); Vasiliev et al. (2015)).

We have presented only one multi-scale simulation due to the high computational cost that such calculations entail. In order to understand how general is this result we revisited coalescence times obtained by a large suite of N-body simulations in Khan et al. (2012b). We rescale[7] their merger product with the one obtained in our cosmological study. We find SMBH merger timescales from the time of binary formation in the range $10-30$ Myr, which satisfactorily match our results. This suggests that the timescale is primarily determined by the characteristic density of the host in the nucleus. Since the stellar mass, $M_\star \lesssim 10^{11}$ M$_\odot$, and the effective radius, $r_{\rm eff} \approx 600$ pc, of our galaxy are typical of observed $z \gtrsim 2$ massive early-type galaxies, we conclude that SMBH mergers in those systems at $z > 2$ should be generically as fast as we find here.

In turn, the scaling argument suggests that the much longer coalescence timescales, of order a Gyr, should be the norm for massive, less dense early-type galaxies at low redshift. These are the galaxies hosting SMBHs with masses $> 10^8$ M$_\odot$, whose mergers should be detectable by Pulsar Timing Arrays (PTAs; Hobbs et al. 2010). Recently, it has been argued that the lack of detection by PTAs might be difficult to reconcile with simple analytical predictions of the hardening rate which assume full loss cone and yield short SMBH merging timescales $\lesssim 10^8$ yr (Shannon et al. 2015). However, here we argue that such short coalescence timescales would occur only at high redshift, hence outside the observability window of PTAs. At low redshift, coalescence times are of order of Gyr; the preceding galaxy merger phase up to SMBH binary formation will also be delayed as major mergers become more rare, with less than 1 merger per galaxy per Gyr expected below $z = 1$ for $L > L^\star$ galaxies (Stewart et al. 2009). Such a low merger rate would likely yield a GW background signal below the detection limit of PTAs, naturally explaining the current lack of detection.

Nevertheless, early-type galaxies with properties expected for a recent dry merger (e.g. shells, tidal tails, and little recent SF) could be the ideal target for detecting SMBH binaries. The fast coalescence times that we find support optimistic expectations for the number of GW emission events detectable with eLISA, at least for the most massive SMBHs in its detection window ($z \sim 2-6$), in the range $10^6 - 10^8$ M$_\odot$. The forecasts assume nearly instantaneous SMBH mergers after the galaxies merge (Amaro-Seoane et al. 2013). Indeed, based on the known scaling relations, the host galaxies of such black holes should have stellar masses above $10^9 - 10^{11}$ M$_\odot$, the mass range at which SF is most efficient in galaxies, yielding dense, triaxial merger remnants that would assist the prompt coalescence of their SMBHs.

We thank Robert Feldmann for providing us with the Argo simulation snapshots. We thank Pedro R. Capelo and Alberto Sesana for useful discussions and for a thorough reading of the manuscript. We thank Rainer Spurzem for support through the Silk Road Project at National Astronomical Observatories of Chinese Academy of Sciences. F.M.K. acknowledges support by the Excellenzinitiative II "Mobilitätsmaßnahmen im Rahmen internationaler Forschungskooperationen 2015-16" of Heidelberg University. D.F. is supported by the Swiss National Science Foundation under grant #No. 200021_140645. P.B. is supported by the Strategic Priority Research Program "The Emergence of Cosmological Structure" of the Chinese Academy of Sciences (No. XDB09000000), the Sonderforschungsbereich SFB 881 "The Milky Way System" (subproject Z2) of the German Research Foundation (DFG)and by the NASU under the Main Astronomical Observatory GRID/GPU computing cluster project.

APPENDIX

NUMERICAL TESTS OF THE PARTICLE SPLITTING

We discuss convergence tests that we have performed in order to assess the numerical impact of the particle splitting. We argue that this procedure perturbs the system only mildly and without altering the SMBH dynamics, as already shown in previous work (Mayer et al. 2007; Roškar et al. 2015). We run other two simulations of the galaxy merger phase at lower spatial resolution; we use a gravitational softening of 15 and 50 pc for stars, gas and SMBHs. The upper row of Figure 6 shows the combinend effect of particle splitting and of introducing the SMBHs at the galaxy centers. Compared to the original cosmological simulation, the galaxies quickly re-adjust their density and velocity dispersion, steepening toward the center. This happens in a few Myr of evolution from the particle splitting; afterwards, they remain stable. This is a natural effect since we add a new gravitational component and we increase the resolution. Nonetheless, it is important to note that outside ~ 2 original softenings of Argo ($2\epsilon = 240$ pc), the profiles do not change much, at least within ~ 10 Myr after the particle splitting, before than the galaxies start to strongly interact

[7] This rescaling is possible because the models by Khan et al. (2012b) are scale-free and physical scaling can be obtained by comparing some characteristic length and mass of the model, e.g. influence radius and mass of SMBH to some reference values.

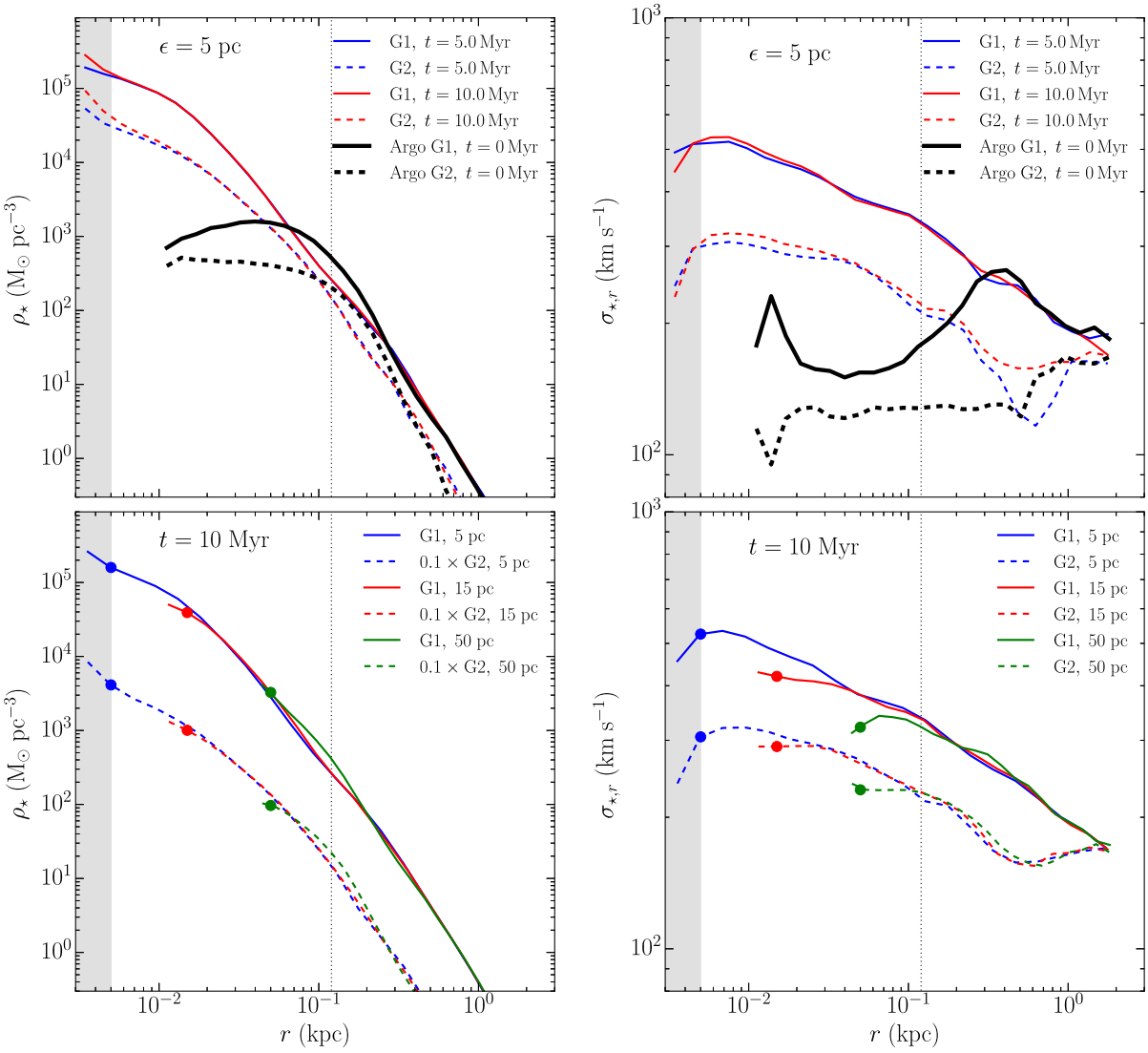
ϵ = 5 pc
G1, t = 5.0 Myr
G2, t = 5.0 Myr
G1, t = 10.0 Myr
G2, t = 10.0 Myr
Argo G1, t = 0 Myr
Argo G2, t = 0 Myr
t = 10 Myr
G1, 5 pc
0.1 × G2, 5 pc
G1, 15 pc
0.1 × G2, 15 pc
G1, 50 pc
0.1 × G2, 50 pc
G2, 5 pc
G2, 15 pc
G2, 50 pc
ρ⋆ (M⊙ pc−3)
σ⋆,r (km s−1)
r (kpc)

Figure 6. Left and right columns show the stellar density and radial velocity dispersion profiles, respectively. Upper row: evolution of the profiles of the central galaxy (G1, continuous lines) and the companion (G2, dashed lines) in the high resolution (5 pc) simulation at different times. Thick lines (i.e. $t = 0$ Myr after particle splitting) shows the profile of the same galaxies in the original Argo simulation. Lower row: comparison of the profiles of the central galaxy (G1, continuous lines) and the companion (G2, dashed lines, decreased by a factor of 10 in $\rho_\star$ for clarity) after 10 Myr from simulations at different resolutions, namely 5 (red), 15 (green), and 50 (blue) pc. The bullets indicate the softening of each run. In all panels, the grey region marks 5 pc, while the vertical dotted line 120 pc.

with each other. This means that the particle splitting and the inclusions of the SMBHs do not introduce spurious effects on scales larger than expected. The lower row of Figure 6 compares the density and velocity dispersion profiles at different numerical resolutions after the initial transient (i.e. 10 Myr after the particle splitting). The profiles at different resolution mutually match each other outside ~ 2 times their own softening. This clearly shows that the particle splitting is robust, at least down to the spatial resolution that we use in our production run.

As a final demonstration that the numerical procedure does not impact on our results, specifically on the SMBH dynamics, we compare in Figure 7 the evolution of the SMBH separation at different resolutions. The SMBH separation is the same until the first pericenter; afterwards, the worse resolution case (50 pc) starts to deviate because the first pericenter occurs at a separation of ~ 4 softening lengths (gravity becomes Newtonian outside 2 softening lengths). Instead, for better resolutions (i.e. smaller softening lengths), the SMBH dynamics converges until the separation reaches again ~ 4 softening lengths. This is also because at higher resolution we can better resolve the formation of the stellar cusp around the SMBHs and their influence radii. In fact, in order to start a new, direct N-body simulation from the re-sampled merger, we use data at $t \sim 21.5$ Myr after the particle splitting, when simulations at different resolutions (at least 15 and 5 pc) converge and the different resolutions do not have an appreciable effect.

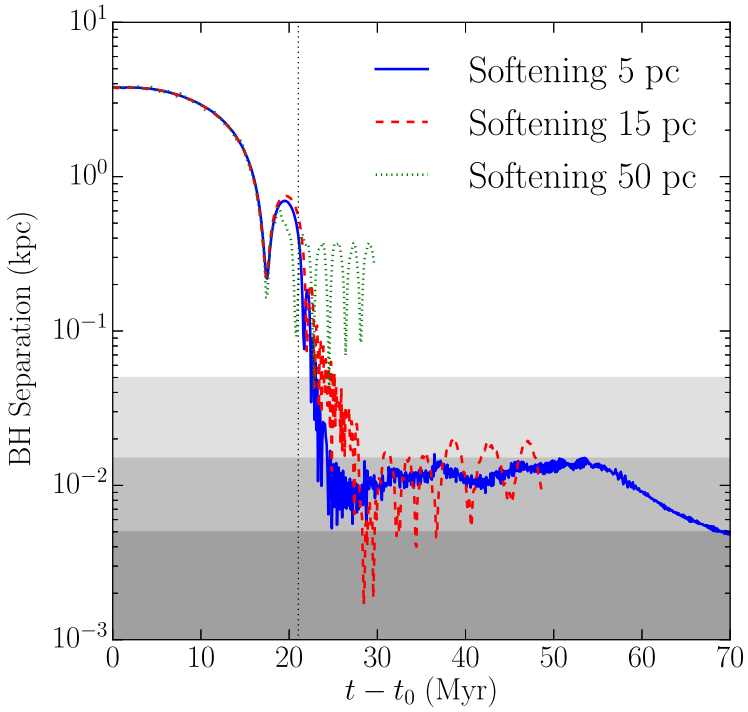

Figure 7. Evolution with time of the separation between the two black holes at different spatial resolution in the re-sampled hydrodynamical simulations of the merger. Blue solid, red dashed, and green dotted lines refer to $\epsilon = 5$, 15 and 50 pc, respectively. The same separations are also marked by the grey shaded bands, while the vertical line indicates the moment at which we initialize the direct N-body simulation.

REFERENCES

Amaro-Seoane, P., Aoudia, S., Babak, S., et al. 2013, GW Notes, Vol. 6, p. 4-110, 6, 4
Begelman, M. C., Blandford, R. D., & Rees, M. J. 1980, Nature, 287, 307
Berczik, P., Merritt, D., & Spurzem, R. 2005, ApJ, 633, 680
Berczik, P., Merritt, D., Spurzem, R., & Bischof, H.-P. 2006, ApJL, 642, L21
Berczik, P., Nitadori, K., Zhong, S., et al. 2011, in International conference on High Performance Computing, Kyiv, Ukraine, October 8-10, 2011., p. 8-18, 8–18
Bezanson, R., van Dokkum, P. G., Tal, T., et al. 2009, ApJ, 697, 1290
Bezanson, R., van Dokkum, P. G., van de Sande, J., et al. 2013, ApJL, 779, L21
Blanchet, L. 2006, Living Reviews in Relativity, 9, 4
Chapon, D., Mayer, L., & Teyssier, R. 2013, MNRAS, 429, 3114
Comerford, J. M., Schluns, K., Greene, J. E., & Cool, R. J. 2013, ApJ, 777, 64
DeGraf, C., Di Matteo, T., Treu, T., et al. 2015, MNRAS, 454, 913
Dotti, M., Colpi, M., Haardt, F., & Mayer, L. 2007, MNRAS, 379, 956
Eracleous, M., Boroson, T. A., Halpern, J. P., & Liu, J. 2012, ApJS, 201, 23
Feldmann, R., Carollo, C. M., Mayer, L., et al. 2010, ApJ, 709, 218
Feldmann, R., & Mayer, L. 2015, MNRAS, 446, 1939
Ferrarese, L., & Merritt, D. 2000, ApJL, 539, L9
Fiacconi, D., Feldmann, R., & Mayer, L. 2015, MNRAS, 446, 1957
Fiacconi, D., Mayer, L., Roškar, R., & Colpi, M. 2013, ApJL, 777, L14
Governato, F., Brook, C., Mayer, L., et al. 2010, Nature, 463, 203
Graham, M. J., Djorgovski, S. G., Stern, D., et al. 2015, Nature, 518, 74
Guedes, J., Callegari, S., Madau, P., & Mayer, L. 2011, ApJ, 742, 76
Hills, J. G. 1983, AJ, 88, 1269
Hobbs, G., Archibald, A., Arzoumanian, Z., et al. 2010, Classical and Quantum Gravity, 27, 084013
Holley-Bockelmann, K., & Khan, F. M. 2015, ApJ, 810, 139
Khan, F. M., Berentzen, I., Berczik, P., et al. 2012a, ApJ, 756, 30
Khan, F. M., Holley-Bockelmann, K., Berczik, P., & Just, A. 2013, ApJ, 773, 100
Khan, F. M., Just, A., & Merritt, D. 2011, ApJ, 732, 89
Khan, F. M., Preto, M., Berczik, P., et al. 2012b, ApJ, 749, 147
Khochfar, S., & Burkert, A. 2006, A&A, 445, 403
Kormendy, J., & Ho, L. C. 2013, ARA&A, 51, 511
Makino, J., & Funato, Y. 2004, ApJ, 602, 93
Mayer, L. 2013, Classical and Quantum Gravity, 30, 244008
Mayer, L., Kazantzidis, S., Madau, P., et al. 2007, Science, 316, 1874
McConnell, N. J., & Ma, C.-P. 2013, ApJ, 764, 184
Merloni, A., Bongiorno, A., Bolzonella, M., et al. 2010, ApJ, 708, 137
Milosavljević, M., & Merritt, D. 2001, ApJ, 563, 34
Papovich, C., Labbé, I., Quadri, R., et al. 2015, ApJ, 803, 26
Peters, P. C., & Mathews, J. 1963, Physical Review, 131, 435
Preto, M., Berentzen, I., Berczik, P., & Spurzem, R. 2011, ApJL, 732, L26
Quinlan, G. D. 1996, New A, 1, 35
Roškar, R., Fiacconi, D., Mayer, L., et al. 2015, MNRAS, 449, 494
Scott, N., Graham, A. W., & Schombert, J. 2013, ApJ, 768, 76
Sesana, A., & Khan, F. M. 2015, MNRAS, 454L, 66
Shannon, R. M., Ravi, V., Lentati, L. T., et al. 2015, Science, 349, 1522
Spaans, M., & Silk, J. 2000, ApJ, 538, 115
Stewart, K. R., Bullock, J. S., Barton, E. J., & Wechsler, R. H. 2009, ApJ, 702, 1005
Szomoru, D., Franx, M., & van Dokkum, P. G. 2012, ApJ, 749, 121
Trakhtenbrot, B., Urry, C. M., Civano, F., et al. 2015, Science, 349, 168
Tremaine, S., Gebhardt, K., Bender, R., et al. 2002, ApJ, 574, 740
Vasiliev, E., Antonini, F., & Merritt, D. 2015, ApJ, 810, 49
Wadsley, J. W., Stadel, J., & Quinn, T. 2004, New A, 9, 137
Wisnioski, E., Förster Schreiber, N. M., Wuyts, S., et al. 2015, ApJ, 799, 209